Real-Time Two-Dimensional Blood Flow Imaging Using an Autocorrelation Technique

CHIHIRO KASAI, KOROKU NAMEKAWA, AKIRA KOYANO, AND RYOZO OMOTO

Abstract—**A new blood flow imaging system is described that combines a conventional pulsed Doppler device and a newly developed autocorrelator. In the system blood flow within a given cross section of a live organ is displayed in real time. The direction of blood flow and its variance are expressed by means of a difference in color and its hue, respectively. Experiments were conducted with a mechanical and an electrical scanner using phantoms, and good agreement with the theory was obtained. Studies on clinical significance have also been carried out for normal and diseased hearts, and successful results have been found.**

I. Introduction

THE TOMOGRAPHIC IMAGING that employs ultrasonic echoes has achieved outstanding advances in recent years, and today ultrasonic diagnostic equipment has become an absolutely indispensable tool for clinical use.

In the meantime the feasibility of measuring blood flow in the heart and vessels using the Doppler effect in ultrasonic waves has become well known. With respect to the method of blood flow measurement, there are two kinds: continuous wave Doppler and pulse wave Doppler, or the so-called pulsed Doppler. Since the pulsed Doppler is capable of providing blood flow information at any depth on the sound beam axis simultaneously with *B*-mode and *M*-mode images, it is widely used at the present time.

The pulsed Doppler system, however, has the disadvantage that only information within a narrow range of the sampling site on the beam axis is obtained. In order to acquire an entire axis flow profile, a multichannel method that employs an increased number of pulsed Doppler sampling gates [1], [2], [3] and the MTI (moving target indication) method [4], [5], [6] have been reported.

Conversely, systems have been devised in which the ultrasonic beam is scanned in a certain cross section for two-dimensional mapping of blood flow [7], [8], [9]. However, the images obtained by the systems are still images, and no real-time observation of actual flow dynamism has been possible.

We have previously developed equipment that displays blood flow movements on a cross section of the heart or blood vessels by the use of an autocorrelation technique in real time, and we have already disclosed its outline [10], [11]. In this paper we describe the details of its principle and the instrumentation. Clinical evaluation of data collected in a hospital is also presented.

Manuscript received March 6, 1984; revised September 7, 1984.

C. Kasai, K. Namekawa, and A. Koyano are with Aloka Company, Ltd., 6-22-1 Mure, Mitaka, Tokyo 181, Japan.

R. Omoto is with Saitama Medical School, Moroyama, Saitama 350-04, Japan.

II. Principle

In the well-known *B*-mode instruments, only the amplitudes of echoes reflected at tissues are imaged. However, in blood flow visualization, the frequency change or phase shift as well as the amplitude of echoes returning from corpuscles must be detected.

Important aspects that provide the flow information effective for diagnosis are 1) flow direction, 2) mean flow velocity, and 3) flow turbulence.

A. Flow Direction

In the pulse echo instrument employing one ultrasonic transducer, the flow component on the sound beam axis is measured. By detecting the polarity of the Doppler frequency shift of echoes with respect to the frequency transmitted, the flow direction (i.e., forward flow or reverse flow) is discriminated.

B. Mean Flow Velocity

Mean blood flow velocity is estimated from the frequency spectra of echoes. When a sound with an angular frequency of ω_0 is transmitted into blood, the received echo signal $e(t)$ from the blood is described as follows [12]:

$$e(t) = R_e \{z(t)e^{j\omega_0 t}\} \tag{1}$$

where $z(t)$ is the complex envelope signal of $e(t)$ and described as

$$z(t) = x(t) + jy(t). \tag{2}$$

Using a quadrature detector the real and imaginary parts of (2) are separately obtained [13]. Denoting the power spectrum of $z(t)$ with $P(\omega)$, the mean angular frequency of $P(\omega)$ is expressed as [12]

$$\bar{\omega} = \frac{\int_{-\infty}^{\infty} \omega P(\omega)\, d\omega}{\int_{-\infty}^{\infty} P(\omega)\, d\omega}. \tag{3}$$

Equation (3) gives the mean Doppler frequency shift due to the blood flow. The mean blood flow velocity $\bar{v}$ is esti-

0018-9537/85/0500-0458$01.00

mated by the following equation [13]:

$$\bar{v} = \frac{\bar{\omega}}{\omega_0} \cdot \frac{c}{2 \cos \theta} \tag{4}$$

where c is the velocity of sound and θ the angle between the sound beam and the blood flow vector.

In the usual ultrasonic diagnostic instrument, the carrier frequency $f_0 = \omega_0/2\pi$ is approximately in the range of 2–5 MHz, and the Doppler frequency $f = \omega/2\pi$ is normally less than 20 kHz.

C. Flow Turbulence

The extent of turbulence in blood flow may be inferred from the variance of the spectrum [14]. Since the Doppler frequency directly relates to the flow vector (i.e., flow direction and speed) in an ultrasonic sample volume, the spectrum spread broadens in accordance with flow disturbance. While in a laminar flow, the spectrum spread is narrow, since a uniform flow vector gives a singular Doppler-frequency shift.

Denoting the standard deviation of the spectrum with σ, the variance σ^2 may be represented by the following [13]:

$$\sigma^2 = \frac{\int_{-\infty}^{\infty} (\omega - \bar{\omega})^2 P(\omega)\, d\omega}{\int_{-\infty}^{\infty} P(\omega)\, d\omega} = \overline{\omega^2} - (\bar{\omega})^2. \tag{5}$$

Now we will find a way to measure the mean angular frequency and its variance using the autocorrelation function of the complex signal $z(t)$. By denoting the autocorrelation function with $R(\tau)$, the following relationship will pertain between $R(\tau)$ and $P(w)$ due to the Wiener–Khinchine's theorem:

$$R(\tau) = \int_{-\infty}^{\infty} P(\omega) e^{j\omega\tau}\, d\omega. \tag{6}$$

Expressing the primary and secondary differentials respectively with $\dot{R}(\tau)$ and $\ddot{R}(\tau)$ of $R(\tau)$ by τ, the following equations are derived from (4), (5), and (6):

$$j\bar{\omega} = \frac{\dot{R}(0)}{R(0)} \tag{7}$$

$$\sigma^2 = \left\{\frac{\dot{R}(0)}{R(0)}\right\}^2 - \frac{\ddot{R}(0)}{R(0)}. \tag{8}$$

It is, of course, possible to measure the mean Doppler frequency and the variance using (7) and (8). However, the direct computation of the equations is rather time-consuming in an actual instrument. Therefore, we will find a simpler method.

When the autocorrelation function is treated as

$$R(\tau) = |R(\tau)| e^{j\phi(\tau)} \tag{9}$$

the following approximation are derived (given in the Appendix):

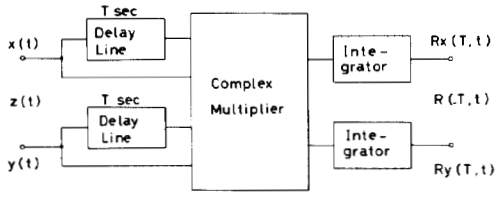

Fig. 1. Complex autocorrelator for calculating $R(T)$.

$$\bar{\omega} = \dot{\phi}(0) = \frac{\phi(T)}{T} \tag{10}$$

$$\sigma^2 = \frac{1}{T^2}\left\{1 - \frac{|R(T)|}{R(0)}\right\} \tag{11}$$

where T denotes the emission interval of ultrasonic pulses. Equations (10) and (11) demonstrate the feasibility of obtaining the mean angular frequency and its variance from autocorrelation values and phases at $\tau = 0$ and $\tau = \mathrm{T}$.

Fig. 1 shows the circuit of a complex autocorrelator for the real-time computation of $R(T)$ and $\phi(T)$. A pair of complex Doppler signals in (2) are split in two, and they are fed to a conjugate complex multiplier, where each of the two signals are input directly, and the other two are supplied via a pair of delay lines with a delay time T. The conjugate complex multiplier executes the following computation

$$z_1(t) = z(t) \times z^*(t - T) \tag{12}$$

where

$$z^*(t - T) = x(t - T) - jy(t - T) \tag{13}$$

is the conjugate complex of function $z(t)$ that has been delayed by time duration T.

The autocorrelation is obtained by integrating $z_1(t)$ for a certain time duration. Thus

$$R(T, t) = \int_{t-nT}^{t} z_1(t')\, dt'$$

$$= R_x(T, t) + jR_y(T, t) \tag{14}$$

$$|R(T, t)| = \sqrt{R_x^2(T, t) + R_y^2(T, t)} \tag{15}$$

where n is the successive number of sound pulses transmitted in the same direction, and hence nT becomes the integration time for a one-beam direction.

The phase ϕ is obtained as the argument of $R(T, t)$

$$\phi(T, t) = \tan^{-1} \frac{R_y(T, t)}{R_x(T, t)}. \tag{16}$$

As understood in (16), the output of the autocorrelator is a function of time t and relates to the integration duration nT. The longer the duration of the integration duration, the better the correlation becomes. This means that better flow images with lesser noises are obtained for a longer integration time.

However, there is a limitation in an actual system, since the frame rate of B-mode images or the field of view is

reduced according to the extension of the integration time. The following equation gives the relationship between the values

$$nTNF = 1 \tag{17}$$

where N is the number of raster lines composing one frame image, and F is the frame-rate per second. For example, when $N = 50$, $F = 15$, the integration time is derived as $nT = 1.33$ ms. If one takes 10 cm of diagnostic depth (i.e. $T = 130$ μs), ten ultrasonic pulses ($n = 10$) can be successively transmitted in each sound beam direction.

While in M-mode, the integration time can be increased to a longer value (say 6–10 ms), and hence a better flow image is obtained since the transmitting sound beam stays in a fixed direction.

In addition, the autocorrelation value for $\tau = 0$ is easily derived by the following equation:

$$R(0, t) = \int_{t-nT}^{t} z(t')z^*(t')\, dt'$$

$$= \int_{t-nT}^{t} \{x^2(t') + y^2(t')\}\, dt'. \tag{18}$$

Thus the blood flow velocity is obtained using (4), (10), and (16), and the variance is with (11), (15), and (18).

III. System

Described below is the two-dimensional blood flow mapping system that employs the subject autocorrelator.

Fig. 2 shows a block diagram of the system, which is equipped with a conventional B-mode imaging unit and a one sample point pulsed-Doppler unit provided with an fast Furrier transform (FFT) spectrum analyzer. Images obtained by these units and flow mapping images are displayed simultaneously and superimposed.

The oscillator (OSC) is a high-frequency oscillator in which the output is divided to provide the clock pulses that trigger various units and the continuous wave that is required for the demodulation of Doppler signals.

Signals received through the transducer are first amplified by a pre-amplifier and a high-frequency amplifier and then conveyed to a pair of quadrature detectors, where the phases of the mixing reference frequency differ by 90°. Since this reference frequency is made identical to that of the transmitting burst wave, the outputs from the low-pass filter (LPF) become the complex Doppler frequencies that have been shifted by Doppler effects, and the pair of outputs also become complex signals with phases that differ by 90°. The pair of signals, after conversion to digital signals by analog-digital (A/D) converters, are passed through delay line cancelers (DLC) [15] and then are supplied to the complex autocorrelator described in Fig. 1.

The delay line cancelers are low-frequency rejection filters that eliminate large echo signals from stationary or slowly moving tissues, which respectively have a zero or low Doppler frequency shift. In the autocorrelator, a sweep video integrator [15] is used to integrate correlated signals. The integration time is changed according to the display mode (i.e., B-mode or M-mode). Its output is conveyed to the velocity calculator and the variance calculator that respectively calculate the mean value and the variance of Doppler signals. The outcome is recorded in a digital scan converter (DSC). The DSC additionally records the B-mode or M-mode images that have been obtained with conventional equipment and FFT-analyzed spectra of the blood flow at any sampling point specified.

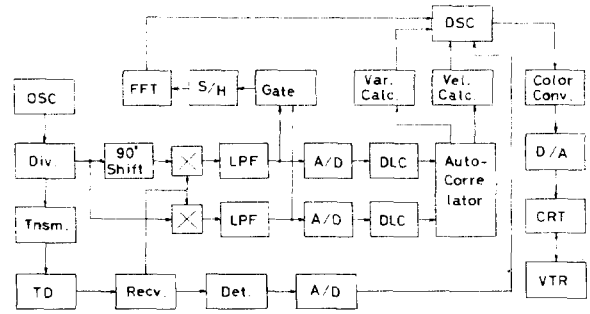

Fig. 2. Block diagram of real-time blood-flow mapping system.

The color converter serves the purpose of converting the data stored in the DSC to chrominance signals. Firstly, with regard to the phase $\phi(T, t)$ that has been obtained with the velocity calculator, the color converter gives red if it is in the first and second quadrants (i.e., $0° < \phi < 180°$). This signifies that the Doppler frequency shift is positive, and therefore the blood flows toward the transducer. If the phase is in the third and fourth quadrants (i.e., $-180° < \phi < 0°$), the color converter gives blue. This signifies that the Doppler frequency shift is negative, and the blood flows away from the transducer. The faster the blood flow, the brighter the color becomes.

Secondly, with regard to the variance, the larger its value, the greater the green blend ratio. Since variance represents the flow turbulence, the color hue changes according to its extent; that is, the red approaches yellow, and blue approaches cyan.

On the other hand, B-mode image, M-mode image, and FFT-analyzed blood-flow data are all converted to black/white as in the conventional way.

The output from the color converter is transformed to analog signals by a D/A converter and is displayed on a color TV screen in real time.

IV. Experiments

Experiments were conducted to examine the performance capabilities of the equipment. The transmitting frequency of the transducer was 3 MHz, and the pulse repetition frequency was 4.4 kHz. The frame rate was 15 frames per second for 40° of the scan angle used.

First, a thread was obliquely stretched across two pulleys placed in a water tank, and the inclination was set such that the angle between the thread and the ultrasonic beam was approximately 60°. A motor was coupled to one of the pulleys to enable the thread to move at any speed desired.

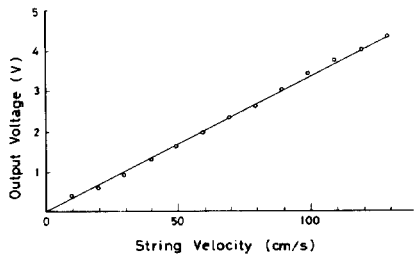

Fig. 3. Output voltage of velocity calculator versus string velocity.

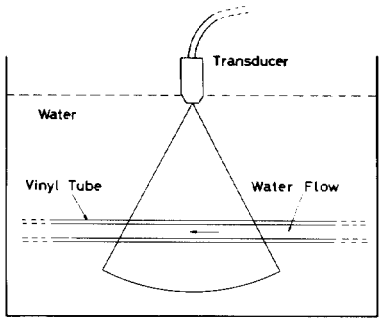

Fig. 4. Experimental setup for the color mapping of flow.

Fig. 3 shows the relationship between the speed of the thread movements and the output from the velocity calculator. The graph indicates that the output voltage of the autocorrelator increases almost linearly, over the entire range examined of the moving speed of the thread, up to 130 cm/s. This demonstrates that the autocorrelator is functioning properly.

Next, to study the relationship between moving objects and the colors on the TV monitor, a vinyl tube was laid horizontally inside the tank as shown in Fig. 4, and tap water was made to flow through it. The ultrasonic beam was scanned in a two-dimensional sector form. In the experiment, tiny bubbles existing in the water may form echo sources.

Fig. 5 shows the *B*-mode color image that was displayed on the TV screen. The image shows no coloring in the central part of the vinyl tube, where ultrasonic waves are incident almost at right angles with the water flow, therefore Doppler frequency shifts do not occur. However in the other portions of the tube, colors are displayed. Since water is flowing from right to left, the color at the right side is red and that at the left side is blue. Owing to the slight turbulence, there is some mixed green. It is also recognized that the color brightness increases according to the distance from the central part due to the increase of Doppler frequency.

Now we will refer to the detectable sensitivity or the signal-to-noise ratio of the system. This stipulation is fairly difficult in actual practice, since various factors are complicatedly related such as flow velocity, the angle between the flow and the sound beam, acoustic attenuation in a medium, integration time of the autocorrelator, sound frequency, transmitted sound power, the sound field of a transducer, etc. In the experiment with water flow described earlier, the signal-to-noise ratio was more than 20 dB for *B*-mode (n = 8, $\theta = 80°$) and about 30 dB for *M*-mode ($n = 64$). However, the ratios are decreased about by 10 dB due to the higher acoustic attenuation and the reverberation in an organ when the system is applied in clinical use, which will be described in the following section.

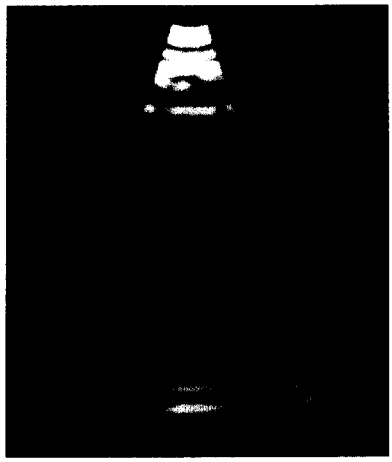

Fig. 5. Color-coded velocity mapping of water flow in a vinyl tube. The forward and backward flows are shown as blue and red-yellow, respectively.

V. Clinical Tests

In this section the clinical data that have been obtained by applying the equipment to the mapping of blood flow within the heart are presented. Fig. 6 is an example that shows blood flow mapping for the long axis crosssection of the heart of a normal subject. Fig. 6(a) is a *B*-mode diastolic image, where the inflow from the left atrium to the left ventricle is displayed in red. Fig. 6(b) is an image in systole where the outflow from the left ventricle to the aorta is displayed in blue.

Fig. 8 is an *M*-mode Doppler display for the normal subject obtained with the ultrasonic beam fixed in the direction of the mitral valve. The difference in blood flow directions in diastole and systole may be interpreted readily from the variations in color.

Fig. 7 shows a diastolic and systolic image of a patient suffering from combined mitral regurgitation and stenosis. Due to the stricture of the valve, the inflow in diastole shows a fast turbulent flow. In systole, on the other hand, a regurgitant flow returning from the left ventricle to the atrium is also observed simultaneously alongside the outflow into the aorta. A comparison of the colors in the outflow with those of the regurgitant flow reveals the regurgitant flow to be more turbulent. This situation may also be understood from the *M*-mode Doppler display in Fig. 9.

X-ray angiographic photographs have also been taken of this case, and their agreement with the Doppler mapping using the equipment under investigation has been verified.

VI. Conclusion

The principle and operation of equipment for observing two-dimensional blood flow in heart and blood vessels in

(a) (b)

Fig. 6. *B*-mode flow images in the heart of a normal patient (a) In diastole inflow is shown in red. (b) In systole outflow is shown in blue.

(a) (b)

Fig. 7. The *B*-mode blood-flow images in the heart of a patient with a valvular disease of mitral regurgitation and stenosis. (a) In diastole high-speed turbulent inflow is shown in red-yellow. (b) In systole regurgitation with turbulence as well as outflow are shown in blue.

Fig. 8. The *M*-mode Doppler display of the normal patient in Fig. 6. The outflow and inflow are shown in blue and red-yellow, respectively.

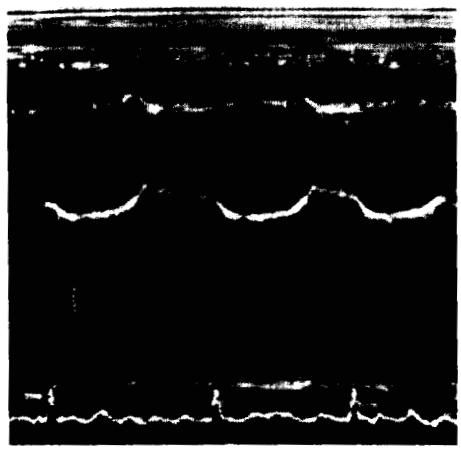

Fig. 9. The *M*-mode Doppler display of the patient with the valvular disease in Fig. 7.

real time have been described. This was accomplished by processing Doppler signals with an autocorrelation technique.

Experiments were conducted by the use of simulators, and the system with the autocorrelator has been verified as operating correctly and properly.

The equipment has been used to treat hospital patients suffering from heart disease, and the two-dimensional mapping of blood flows in the heart has been performed. The results have verified the feasibility of the equipment in the clinical field as valvular diseases, septum defects, and other diseases are diagnosed quite easily and noninvasively from the real-time two-dimensional information of blood flow.

APPENDIX

Defining

$$R(\tau) = |R(\tau)|\, e^{j\phi(\tau)} = A(\tau)e^{j\phi(\tau)} \tag{A1}$$

and considering that $A(\tau)$ is an even function and $e^{j\phi(\tau)}$ an odd function, we find

$$\dot{R}(\tau) = (\dot{A}(\tau) + jA(\tau)\,\dot{\phi}(\tau))e^{j\phi(\tau)} \tag{A2}$$

therefore

$$\dot{R}(0) = jA(0)\,\dot{\phi}(0) \tag{A3}$$

$$R(0) = A(0) \tag{A4}$$

From (4), (A3) and (A4), we find

$$\bar{\omega} = \dot{\phi}(0) \cong \{\phi(T) - \phi(0)\}/T = \phi(T)/T \tag{A5}$$

where T is the emission interval of ultrasonic pulses, during which we assume approximately constant velocity of movements of the reflective bodies. By differentiating (A2) with τ and inserting $\tau = 0$, we obtain

$$\ddot{R}(0) = -(\dot{\phi}(0))^2 A(0) + \ddot{A}(0). \tag{A6}$$

From (5), (A3), (A4), and (A6), we know

$$\sigma^2 = -\ddot{A}(0)/A(0). \tag{A7}$$

By spreading $A(\tau)$ out in a series relative to τ and considering that $A(\tau)$ is an even function, we find

$$A(\tau) = A(0) + \frac{\tau^2}{2}\ddot{A}(0) + \cdots. \tag{A8}$$

Neglecting the third and later terms of (A8) as small enough in value and using (A6) and (A7) with insertion of $\tau = T$, we obtain

$$\sigma^2 \cong \frac{2}{T^2}\left\{1 - \frac{A(\tau)}{A(0)}\right\} = \frac{2}{T^2}\left\{1 - \frac{|R(T)|}{R(0)}\right\}. \tag{A9}$$

REFERENCES

[1] D. W. Baker, "Pulsed Doppler blood flow sensing," *IEEE Trans. Sonics Ultrason.*, vol. SU-17, no. 3, pp. 170–185, 1970.

[2] P. J. Fish, "Multichannel direction resolving Doppler angiography," in *Proc. 2nd European Congr. on Ultrason. in Medicine*, (Excerpta Medica), pp. 153–159, 1975.

[3] M. Brandestini, "Topflow—A digital full-range Doppler velocity meter," *IEEE Trans. Sonics Ultrason.*, vol. SU-25, no. 5, pp. 287–293, 1978.

[4] P. A. Grandchamp, "A novel pulsed directional Doppler velocimeter, the phase-detection profilometer," in *Proc. 2nd European Congr. on Ultrason. in Medicine* (Excerpta Medica), 1975, pp. 137–143.

[5] M. Brandestini, "Application of the phase detection principle in transcutaneous velocity profile meter," in *Proc. 2nd European Congr. on Ultrason. in Medicine* (Excerpta Medica), 1975, pp. 144–152.

[6] A. Nowicki and J. A. Reid, "An inifinite gate-pulsed Doppler," *Ultrason. in Medicine and Biology*, vol. 7, pp. 41–50, 1981.

[7] G. B. Curry and D. N. White, "Color-coded ultrasonic differential velocity arterial scanner (echo flow)," *Ultrason. in Medicine and Biology*, vol. 4, p. 27, 1978.

[8] B. A. Coghlan and M. G. Taylor, "A carotid imaging system utilizing continuous-wave Doppler-shift ultrasound and real-time spectrum analysis," *Med. & Biol. Eng. & Comp.*, vol. 16, pp. 739–744, 1978.

[9] M. Asao *et al.*, "Flow mapping of intracardiac blood flow by computer-based ultrasonic multigated pulsed Doppler flowmeter," in *Proc. 20th Conf. Japan Soc. of Med. Elect. and Biol. Eng.*, vol. 44, 1981 (in Japanese).

[10] K. Namekawa *et al.*, "Imaging of blood flow using autocorrelation," *Ultrason. in Medicine and Biology*, vol. 8, suppl. 1, 1982.

[11] ——, "Real-time blood flow imaging system utilizing autocorrelation techniques," in *Proc. 3rd Conf. of the World Federation for Ultrason. in Medicine and Biology*, (5th World Congr. of Ultrason. in Medicine and Biology, R. A. Lerski and P. Morley). New York:Pergamon, pp. 203–208, 1982.

[12] B. Angelsen, "Instantaneous frequency, mean frequency, and variance of mean frequency estimators for ultrasonic blood velocity Doppler signals," *IEEE Trans. Biomed. Eng.*, vol. BME-28, no. 11, pp. 733–741, 1981.

[13] L. Hatle and B. Angelsen, *Doppler Ultrasound in Cardiology*. Philadelphia: Lea & Febiger, 1982.

[14] B. Angelsen, "A Theoretical Study of the Scattering of Ultrasound from Blood," *IEEE Trans. Biomed Eng.*, vol. BME-27, no. 2, pp. 61–67, 1980.

[15] M. I. Skolnik, *Radar Handbook*. New York:McGraw-Hill, 1970.

Chihiro Kasai was born in Nagano Prefecture, Japan, on October 2, 1938. He received the B.S., M.S., and Ph.D. degrees in electrical engineering from Tohoku University, Sendai, Japan, in 1962, 1964, and 1974, respectively.

In 1964 he joined the Research Institute of Electrical Communication, Tohoku University, where he was a Research Associate till 1974. In 1974 he moved to Aloka Company, Ltd., Mitaka, Tokyo, where he has been engaged in the research and development of ultrasonic diagnostic equipment. He is now a manager of the Research Institute Division.

Dr. Kasai is a member of the Institute of Electronics and Communication Engineers of Japan, the Acoustical Society of Japan, and the Japan Society of Ultrasonics in Medicine.

Koroku Namekawa was born in Akita, Japan, on May 22, 1917. He received the B.S. degree from the Department of Applied Physics, Tokyo Physical Science College, Japan, in 1940.

He joined Japan Radio Company in 1954, where he was engaged in the research and development of radar system. In 1976 he moved to Aloka Company, Ltd., where he has been engaged in the research and development of ultrasonic diagnostic equipment. His present interests are the processing of ultrasonic Doppler signal and its application to real time blood flow mapping.

Mr. Namekawa is a member of the Institute of Electronics and Communication Engineers of Japan, the Japan Society of Ultrasonics in Medicine, and the Japan Society of Medical Electronics and Biological Engineering.

Akira Koyano was born in Tokyo, Japan on June 16, 1928. He graduated from the department of electrical communication, Waseda Technical School, Tokyo in 1945.

He entered the Research Institute of NEC company in 1945, where he worked as a Research Assistant. In 1950, he moved to Aloka Company, Ltd., where he particiated in the development of radiation instruments until 1978. Since then he has been engaged in the research and development of ultrasonic diagnostic equipment, and he is now a Senior Director.

Mr. Koyano is a member of the Japan Society of Nuclear Medicine and the Japan Society of Ultrasonics in Medicine.

Ryozo Omoto was born in Hokkaido, Japan, on March 10, 1932. He received the M.D. and Ph.D. degrees in 1959 and 1967, respectively, from the University of Tokyo, Japan.

Since 1977 he has been a Professor and Chairman at the Department of Surgery, Saitama Medical School, covering cardiovascular surgery, Saitama, Japan. He worked on new ultrasound techniques in the cardiovascular field. He developed clinically an intra-cardiac scanning method using an intravenous probe in 1962 and first described the clinical application of color flow-mapping in heart diseases with real-time two-dimensional Doppler echocardiography.

Dr. Omoto is a member of the Japanese Society of Surgery, the Japanese Association for Thoracic Surgery, the Japanese Circulation Society, and the Japan Society of Ultrasonics in Medicine.